DOI: 10.13009/EUCASS2023-028
Aerospace Europe Conference 2023 – 10TH EUCASS – 9TH CEAS

Fault-tolerant Orbit and attitude control of Solar sail with a rapid inspection and repair strategy of faulty RCDs

Fuqiang Duan [1], Hongyi Xie [2†] and Franco Bernelli-Zazzera [2]
[1] National University of Defence Technology
109 Deya Road, Changsha 410073, People's Republic of China
duanfuqiang20@nudt.edu.cn
[2] Department of Aerospace Science and Technology, Politecnico di Milano
Via La Masa, 34 20156 Milano, Italy
hongyi.xie@polimi.it – franco.bernelli@polimi.it
[†] Corresponding Author

Abstract

This paper presents a fault-tolerant control method for solar sail spacecraft, aiming to mitigate hazards caused by RCD failures. The study includes modelling the attitude dynamics, classifying the failure of RCDs into 4 different types for quick diagnosis, establishing a control approach that utilizes RCD switch control for recovering the solar sail from the situation of fault, and conducting simulations to verify its effectiveness. Results from simulations involving four fault cases confirm the efficacy of the proposed fault-tolerant control method.

1. Introduction

The continuous advancement of space technology necessitates increasingly stringent functional density and system complexity in space vehicles, enabling them to undertake complex deep space exploration missions and enhance mission execution capabilities. However, this progress also brings a higher risk of system failures [1]. To reduce reliance on ground-based measurement and control, enhance the safety of spacecraft in orbit, and minimize operational costs, autonomous operation in complex environments must be improved, allowing spacecraft to complete missions with maximum autonomy. Achieving these objectives requires space systems with fault tolerance and self-healing capabilities, enabling timely and effective responses to abnormal system conditions, ensuring mission success, and significantly reducing economic losses. Notably, the United States has invested substantial resources in spacecraft fault diagnosis and health management, resulting in a 50% risk reduction and 30% budget reduction [2-3].

The attitude control system, a fundamental and critical subsystem of space systems, is pivotal for the smooth execution of space missions, making it essential to enhance its reliability [2-3]. Unfortunately, the attitude control system is susceptible to failures. According to [4], the failure of control subsystem accounted for 37% of the failures occurred in remote sensing spacecraft between 1988 and 2014. An unknown failure in September 2008 impacted the attitude orbit control system of the US early warning satellite DSP-23, necessitating additional investments by the US Department of Security, but the satellite could not be recovered.

Solar sail spacecraft are more susceptible to actuator failures compared to common satellites. This is primarily due to their extensive use of reflectivity control devices (RCDs) actuators, which utilize liquid crystal (LC) to adjust the reflectivity of sunlight [5]. The large number of actuators increases the probability of faults occurring. Additionally, the unique configuration of RCDs in different positions results in varying attitude control torques and thrust control quantities, making a faulty solar sail even more complex to manage than a typical satellite in a similar situation.

Furthermore, the International Astronomical Society has reported that solar storms will be more active in 2023 and the upcoming years [6]. These intense solar storms pose a greater risk to the RCDs mounted on solar sails due to the strong electromagnetic coupling. As a result, the RCDs are more prone to damage or interruption compared to actuators

DOI: 10.13009/EUCASS2023-028

on traditional satellites. This highlights the urgent need for a fault-tolerant control scheme for solar sails planned to be deployed in the orbit in the coming years. Overall, the unique characteristics of solar sail spacecraft, coupled with the increasing intensity of solar storms, necessitate the development of robust fault-tolerant control schemes to ensure the successful operation of solar sails in the challenging space environment.

However, despite the inherent risk of actuator failure in solar sails with RCDs, to the best knowledge of the authors, no previous research specifically addressing the issue of failed actuators in solar sails. The only existing research related to fault-tolerant control of a sail spacecraft is mentioned in [7], which focused on addressing sensing limitations in an electric sail spacecraft formation, accounting for errors in attitude determination and control subsystems, as well as the potential variability of thrust magnitude resulting from solar wind effects. As a result, there is no direct reference available from previous research. Therefore, the following literature review will be based on current research conducted on other spacecraft, such as nanosatellites.

The application of active and passive fault-tolerant control techniques plays a crucial role in enhancing the robustness and recovery capability of attitude control systems in the presence of in-orbit failures. It ensures high-quality attitude control performance even under failure conditions, considering the uncertainties encountered in space operations and the limited human intervention [8]. Extensive literature [9-10] provides detailed insights into the importance and development status of fault diagnosis and fault-tolerant control techniques for spacecraft attitude control systems. Numerous examples have also demonstrated the effectiveness and necessity of designing fault-tolerant controllers for spacecraft attitude control.

For instance, in on-orbit expansion experiments of the SAX satellite in the late 20th century, it was discovered that a suitable fault-tolerant controller design for the malfunctioning attitude control system ensured the continuation of the satellite mission [11] and met the mission requirements [12]. In situations where the far-UV spectral detector gyroscope exhibits degraded performance and two orthogonal flywheels fail, reconfiguring the fault-tolerant control mechanism using redundant flywheels and magnetic moments enables the recovery of partial attitude control performance [13]. Moreover, in the event of a loss of attitude stability control due to failures caused by space debris impacts, a fault-tolerant controller can be designed using techniques like the Kalman filter to restore attitude control performance [14]. During satellite formation, when faced with magnetic moment device failure and saturation phenomena, the design of a magnetic moment device-based spin stabilization algorithm can achieve attitude stability control [15]. Furthermore, scholars have considered satellite thruster failures and effectively improved the fault tolerance of satellite control systems by combining the optimal table look-up method with linear programming [16]. In [17], a fault-tolerant satellite service management system was designed for the Pi satellite by integrating redundancy, self-diagnosis, and watchdog technology. In conclusion, the development of autonomous and reliable attitude control systems for satellites in orbit necessitates extensive theoretical and technical research on fault-tolerant control. This research is of significant academic value, strategic significance, and application prospects. Strengthening autonomous operation and maintenance capabilities to address the harsh conditions of the outer space environment is a critical objective.

This paper aims to investigate the attitude fault-tolerant control of the attitude actuator in the event of partial damage to the RCDs in a solar sail spacecraft. The second section models the attitude - orbit coupling dynamics of the solar sail spacecraft. The third section analyzes the damage classification of the solar sail spacecraft. The fourth section establishes the fault-tolerant control and analyzes its stability. The fifth section analyzes several cases of different types of damage for simulation calculations. Besides, the last section summarizes the effect of the proposed fault-tolerant control scheme and prospects the further work.

2. Preliminaries

Consider a solar sail situated in the GEO. It is characterized by a flat and perfectly reflective surface with a total reflective area. The solar sail is actuated by the RCDs that composed of several small electrochromic material panels (EMPs). The total area of these EMPs can be modified by applying a suitable electric voltage to adjust their optical coefficients, as depicts in the following Fig. 1, in which the RCDs are represented by the yellow squares as follows:

DOI: 10.13009/EUCASS2023-028

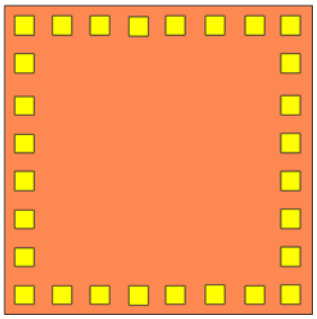

Figure 1: Solar sail schematic

2.1 Spacecraft Attitude Dynamics

The equations of motion in terms of unit-quaternion for the solar sail are given as follows:

$$\boldsymbol{J}\dot{\boldsymbol{\omega}} = \boldsymbol{\omega}^{\times}\boldsymbol{J}\boldsymbol{\omega} + \boldsymbol{D}\boldsymbol{u}_c + \boldsymbol{d} \tag{1}$$

$$\dot{\boldsymbol{Q}} = \frac{1}{2}\begin{bmatrix} S(\boldsymbol{q}) + q_0\boldsymbol{I}_3 \\ -\boldsymbol{q}^T \end{bmatrix}\boldsymbol{\omega}_b \tag{2}$$

where $\boldsymbol{J}\in\boldsymbol{R}_{3\times3}$ represents a symmetric positive-definite inertia matrix, and the vector $\boldsymbol{\omega}\in\mathbf{R}_3$ denotes the angular velocity in the body-fixed frame. The unit-quaternion $\boldsymbol{T}\in\boldsymbol{R}_4$, where $\boldsymbol{Q}=[q_0 \quad q_1 \quad q_2 \quad q_3]^T$, describes the attitude, and the control torque, $u\in\boldsymbol{R}_n$, produced by n actuators about the body axes is represented by the actuator configuration matrix $\boldsymbol{D}\in\boldsymbol{R}_{3\times n}$. Moreover, $d\in\boldsymbol{R}_3$ denotes environmental disturbances. It should be noted that $\boldsymbol{q}$ and q_0 represent the vector and scalar parts, respectively, of the unit quaternion, satisfying $\boldsymbol{q}^T\boldsymbol{q} + q_0^2 = 1$. Additionally, the matrix $\boldsymbol{S}(x)\in\boldsymbol{R}_{3\times3}$ denotes the askew-symmetric matrix corresponding to any vector $x \in \boldsymbol{R}_3$.

2.2 Switchable force models utilizing RCDs

The switchable nature of the SRP force acting on the RCD arises from differences in the optical parameters depending on the voltage applied to it. In the aerospace domain, the SRP force acting on a film can be modeled using Equation (3) as follows:

$$\boldsymbol{F} = P \cdot \Delta s(\boldsymbol{n}_s \cdot \boldsymbol{n})\left[(C_a + C_d)\boldsymbol{n}_s + \left(\frac{2}{3}C_d + 2C_s(\boldsymbol{n}_s \cdot \boldsymbol{n})\right)\boldsymbol{n}\right] \tag{3}$$

Where P represents the solar radiation pressure on the RCD, $\boldsymbol{n}$ means the unit normal direction vector of the RCD surface, $\boldsymbol{n}_s$ represents the unit vector parallel to the sunlight, and Δs is an area element.

Table 1: Theoretical system states of the RCD

	On	**Off**
C_a	0	0
C_d	0	1
C_s	1	0

Table 1 presents two distinct states (ON/OFF) that affect the absorptivity (Ca), diffuse reflectivity (Cd), and reflectivity (Cs) of the RCD. By plugging in the parameter values from Table 1 into Equation (3), it is possible to calculate the SRP force on the RCD as follows:

$$\boldsymbol{F}^{ON} = P \cdot \Delta s(\boldsymbol{n}_s \cdot \boldsymbol{n})^2 \cdot \boldsymbol{n} \tag{4}$$

$$\boldsymbol{F}^{OFF} = P \cdot \Delta s(\boldsymbol{n}_s \cdot \boldsymbol{n})\left(\boldsymbol{n}_s + \frac{2}{3}\boldsymbol{n}\right) \tag{5}$$

DOI: 10.13009/EUCASS2023-028

2.3 Actuator Fault Models

There are 4 possible scenarios of failure that RCDs might meet, each of them has been illustrated as the following Fig. 2 to Fig. 5 depict. In these figures, the RCDs that can continue their normal working are symbolized by the yellow squares, while the failed RCDs are represented by the dark squares.

Failure mode A: Only one of the RCD is failed.

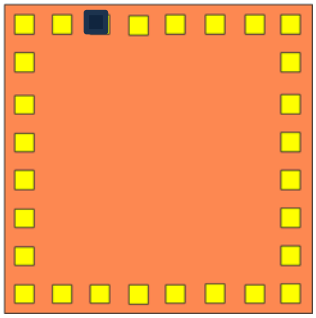

Figure 2: schematic of failure mode A

Failure mode B: multi-RCDs fault and regular RCDs could not output the same torque as faulty RCDs.

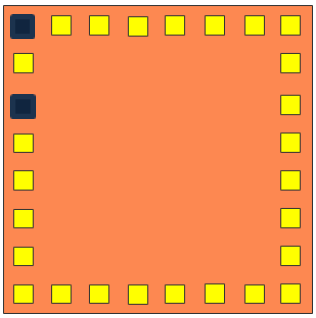

Fig. 3. schematic of failure mode B

Failure mode C: More than one quarter RCDs fault.

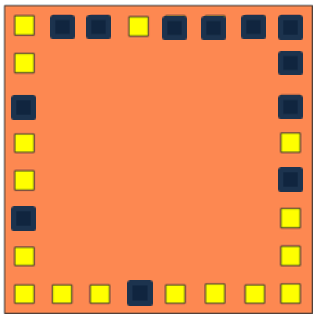

Fig. 4. schematic of failure mode C

DOI: 10.13009/EUCASS2023-028

Failure mode D: multi-RCDs fault and regular RCDs could output the same torque as faulty RCDs.

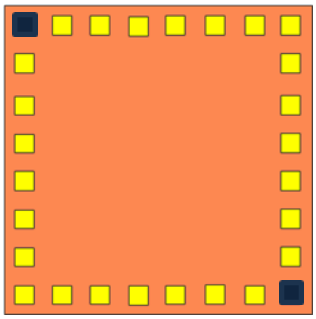

Fig. 5. schematic of failure mode D

Based on the above mentioned 4 possible schemes of RCDs failure, a rapid inspection strategy is proposed in the following section to figure out the positions of the failed RCDs:

3. Rapid Inspection and Recovery Strategy

The following pseudo codes are proposed to judge the classifications of the failure as quickly as possible:

Table 2: Inspection algorithm for judgment number of faulty RCDs

Algorithm 1

Require: $\boldsymbol{D_c}$, $\boldsymbol{u_c}$, $\boldsymbol{F_a}$ ($\boldsymbol{F_a}$ represent the number of faulty RCDs, initial $\boldsymbol{F_a=0}$)

Ensure: switch one of elements in RCDs

if the RCD is ON calculate

$$\boldsymbol{D_c}\left[\sum_{i=1}^{n+1} r_{ix}^{ON} \quad \sum_{i=1}^{n+1} r_{iy}^{ON} \quad \sum_{i=1}^{m-1} r_{ix}^{OFF} \quad \sum_{i=1}^{m-1} r_{iy}^{OFF}\right]^T$$

else calculate

$$\boldsymbol{D_c}\left[\sum_{i=1}^{n-1} r_{ix}^{ON} \quad \sum_{i=1}^{n-1} r_{iy}^{ON} \quad \sum_{i=1}^{m+1} r_{ix}^{OFF} \quad \sum_{i=1}^{m+1} r_{iy}^{OFF}\right]^T$$

for elements in RCDs

if

$$\boldsymbol{D_c}\left[\sum_{i=1}^{n+1} r_{ix}^{ON} \quad \sum_{i=1}^{n+1} r_{iy}^{ON} \quad \sum_{i=1}^{m-1} r_{ix}^{OFF} \quad \sum_{i=1}^{m-1} r_{iy}^{OFF}\right]^T = \boldsymbol{D_c}\left[\sum_{i=1}^{n} r_{ix}^{ON} \quad \sum_{i=1}^{n} r_{iy}^{ON} \quad \sum_{i=1}^{m} r_{ix}^{OFF} \quad \sum_{i=1}^{m} r_{iy}^{OFF}\right]^T$$

or $$\boldsymbol{D_c}\left[\sum_{i=1}^{n-1} r_{ix}^{ON} \quad \sum_{i=1}^{n-1} r_{iy}^{ON} \quad \sum_{i=1}^{m+1} r_{ix}^{OFF} \quad \sum_{i=1}^{m+1} r_{iy}^{OFF}\right]^T = \boldsymbol{D_c}\left[\sum_{i=1}^{n} r_{ix}^{ON} \quad \sum_{i=1}^{n} r_{iy}^{ON} \quad \sum_{i=1}^{m} r_{ix}^{OFF} \quad \sum_{i=1}^{m} r_{iy}^{OFF}\right]^T$$

calculate $\boldsymbol{F_a} = \boldsymbol{F_a} + 1$

end for: ergodic all of the RCDs

$\boldsymbol{F_a}$**=1** represent failure mode A

$\boldsymbol{F_a}$**>(m+n)/4** represent failure mode C

$\boldsymbol{F_a}$**>1 and** $\boldsymbol{F_a}$**≤(m+n)/4** represent failure mode B or D

The inspection strategy proposed in Table 2 can separate the failure mode A and failure mode C from all kinds of RCDs failures. A further search strategy is proposed in the following Table 3 to judge whether the system is under the states in harmony with the case of failure mode B or failure mode D as follows:

DOI: 10.13009/EUCASS2023-028

Table 3: inspection algorithm for judgment failure mode D

Algorithm 2
Require: $\boldsymbol{D_c}, \boldsymbol{u_c}, \boldsymbol{F_a}$
Exist Two or more groups
$\boldsymbol{D_c}\left[\sum_{i=1}^{n+F_a} r_{ix}^{ON} \quad \sum_{i=1}^{n+F_a} r_{iy}^{ON} \quad \sum_{i=1}^{m-F_a} r_{ix}^{OFF} \quad \sum_{i=1}^{m-F_a} r_{iy}^{OFF}\right]^T = \boldsymbol{D_c}\left[\sum_{i=1}^{n} r_{ix}^{ON} \quad \sum_{i=1}^{n} r_{iy}^{ON} \quad \sum_{i=1}^{m} r_{ix}^{OFF} \quad \sum_{i=1}^{m} r_{iy}^{OFF}\right]^T$
or $\boldsymbol{D_c}\left[\sum_{i=1}^{n-F_a} r_{ix}^{ON} \quad \sum_{i=1}^{n-F_a} r_{iy}^{ON} \quad \sum_{i=1}^{m+F_a} r_{ix}^{OFF} \quad \sum_{i=1}^{m+F_a} r_{iy}^{OFF}\right]^T = \boldsymbol{D_c}\left[\sum_{i=1}^{n} r_{ix}^{ON} \quad \sum_{i=1}^{n} r_{iy}^{ON} \quad \sum_{i=1}^{m} r_{ix}^{OFF} \quad \sum_{i=1}^{m} r_{iy}^{OFF}\right]^T$

Meet **Algorithm 2** represent failure mode D
Do not meet **Algorithm 2** represent failure mode B

In view of the above rapid inspection method to classify 4 different kinds of RCDs failure, the fault-tolerant control strategy is proposed in the following part with quite different control parameters selections according to different classified faulty modes.

4. Fault-tolerant Control System

4.1 Deformation of the Dynamics Model

To bring the RCD array to a situation with more controllable, both $\boldsymbol{D}$ and $\boldsymbol{u}$ are deformed as follows:

$$\boldsymbol{Du} = \sum_{i=0}^{n}\begin{bmatrix} 0 & 0 & r_{iy}^{ON} \\ 0 & 0 & r_{ix}^{ON} \\ r_{iy}^{ON} & r_{ix}^{ON} & 0 \end{bmatrix}\begin{bmatrix} u_x^{ON} \\ u_y^{ON} \\ u_z^{ON} \end{bmatrix} + \sum_{i=0}^{m}\begin{bmatrix} 0 & 0 & r_{iy}^{OFF} \\ 0 & 0 & r_{ix}^{OFF} \\ r_{iy}^{OFF} & r_{ix}^{OFF} & 0 \end{bmatrix}\begin{bmatrix} u_x^{OFF} \\ u_y^{OFF} \\ u_z^{OFF} \end{bmatrix} \tag{6}$$

where $r_{ix}^{ON}, r_{iy}^{ON}, r_{iz}^{ON}$ represent the 3-Axis position of RCDs which on mode ON, $r_{ix}^{OFF}, r_{iy}^{OFF}, r_{iz}^{OFF}$ represent the 3-Axis position of RCDs which on mode OFF, And $r_{iz}^{ON} = 0, r_{iz}^{OFF} = 0$. $u_x^{ON}, u_y^{ON}, u_z^{ON}$ represent the force of RCDs output which on mode ON, $u_x^{OFF}, u_y^{OFF}, u_z^{OFF}$ represent the force of RCDs output which on mode OFF. Note that (6) is composed of 2 different multinomials. It's rational to simplify (6) as follows:

$$\boldsymbol{D_c u_c} = \begin{bmatrix} 0 & u_z^{ON} & 0 & u_z^{OFF} \\ u_z^{ON} & 0 & u_z^{OFF} & 0 \\ u_y^{ON} & u_x^{ON} & u_y^{OFF} & u_x^{OFF} \end{bmatrix}\begin{bmatrix} \sum_{i=1}^{n} r_{ix}^{ON} \\ \sum_{i=1}^{n} r_{iy}^{ON} \\ \sum_{i=1}^{m} r_{ix}^{OFF} \\ \sum_{i=1}^{m} r_{iy}^{OFF} \end{bmatrix} \tag{7}$$

where $\boldsymbol{u_c}$ is the designed attitude control torques, and $\boldsymbol{D_c}$ is a matrix to point out the states of all the RCDs fixed on different positions. Then the attitude dynamics of the solar sail can be rewritten as follows:

$$\boldsymbol{J\dot{\omega}} = \boldsymbol{\omega}^{\times}\boldsymbol{J\omega} + \boldsymbol{D_c u_c} + \boldsymbol{d_f} + \boldsymbol{d} \tag{8}$$

where $\boldsymbol{d_f}$ denotes the disturbances led by faulty RCDs, and $\boldsymbol{d}$ denotes the disturbances owing to other factors. Moreover, a sliding-mode vector is given as follows:

$$\boldsymbol{s} = c_1\boldsymbol{\omega} - c_2\boldsymbol{q} \tag{9}$$

DOI: 10.13009/EUCASS2023-028

where c_1 and c_2 represent the control coefficient. To recovery the effective attitude control of the solar sail with failed RCDs, a fault-tolerant attitude controller is proposed as follows:

$$\boldsymbol{u}_c = -\frac{\boldsymbol{u}_{max}}{\varepsilon_0}\boldsymbol{D}^{+}\frac{\boldsymbol{s}}{\|\boldsymbol{s}\|} \tag{10}$$

where ε_0 represents a control coefficient, the selection for the parameter ε_0 is quite different for the solar sail under different modes of RCDs faulty. Usually, higher ε_0 should be selected for a solar sail with more faulty RCDs, but there doesn't exist a definite criterion for the selection of ε_0, which is needed to be investigated in the further work. Moreover, $\boldsymbol{D}^{+}$ denotes the pseudo-inverse of the matrix $\boldsymbol{D}$, and $\boldsymbol{u}_{max}$ represents the control matrix with maximum output torques. Then the Lyapunov candidate can be selected as follows:

$$V = \boldsymbol{q}^T\boldsymbol{q} + \frac{1}{2}\boldsymbol{s}^T\boldsymbol{J}\boldsymbol{s} \tag{11}$$

The corresponding time derivative is calculated as follows:

$$\dot{V} \le \boldsymbol{\omega}^T\boldsymbol{q}_e + \boldsymbol{s}^T\left(-\frac{\boldsymbol{u}_{max}}{\varepsilon_0}\boldsymbol{D}^{+}\frac{\boldsymbol{s}}{\|\boldsymbol{s}\|} + \boldsymbol{f}\right) \le -\|\boldsymbol{q}_e\|^2 - \left(\frac{\|\boldsymbol{u}_{max}\|}{\varepsilon_0} - \|\boldsymbol{f}\|\right)\|\boldsymbol{s}\| \tag{12}$$

It's observed that $\dot{V} \le -\|\boldsymbol{q}_e\|^2 \le 0$ is easy to achieve as long as $\varepsilon_0 \le \|\boldsymbol{u}_{max}\|/\|\boldsymbol{f}\|$, while ε_0 is a design parameter that can be set. Thus, the proposed attitude control system is substantiated to be a Lyapunov stabilized one.

5. Numerical Simulation and Analysis

To validate the effectiveness and performance of the designed Fault Tolerance control scheme, a scenario of solar sail spacecraft fly-around GEO is simulated. The goal is to realize the attitude stabilization of the solar sail spacecraft. In the simulation scenario, the solar sail spacecraft is assumed to be flying in GEO with the parameters set as follows: The semimajor axis a_t = 42164000 m, the orbit eccentricity e_t = 0, the initial true anomaly $v_{(0)}$ = 0 rad, orbit inclination i_t = 0 rad, argument of perigee w_t = 0 rad, and right ascension of ascending node t = 0 rad.

The nominal parts and perturbation terms of the chaser's mass and inertia matrix parameters are given as m_0 = 5 kg, J_0 =[10, 0, 0; 0, 10, 0; 0, 0, 10]kg·m^2. The initial quaternion are set as [0.927,-0.1,0.2,-0.2]^T, with the initial angular velocity set as [0.005,0.006,0.004]^T.

Through FTC, the numerical results of the change of quaternion and angular velocity in 1000s are presented in Figs. 6 to 17. For a solar sail with initial $\boldsymbol{u}_{c0} = [4 \quad 5 \quad 0 \quad 0]^T$ that in accordance with the faulty mode A, the control parameter ε_0 is selected as $\varepsilon_0 = 1$, and the following Figs. 6-7 illustrate its attitude variation with the employment of the proposed control scheme:

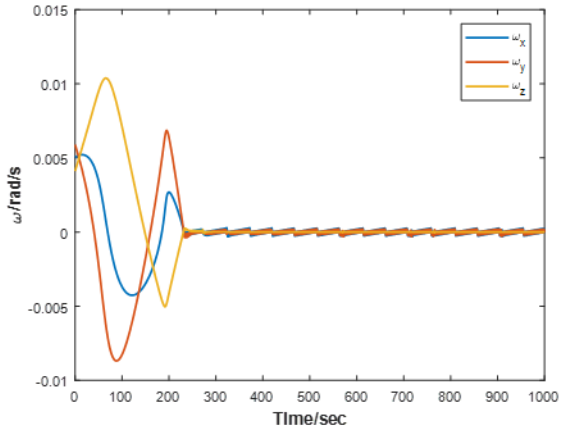

Fig. 6. The angular velocity changes on failure mode A

DOI: 10.13009/EUCASS2023-028

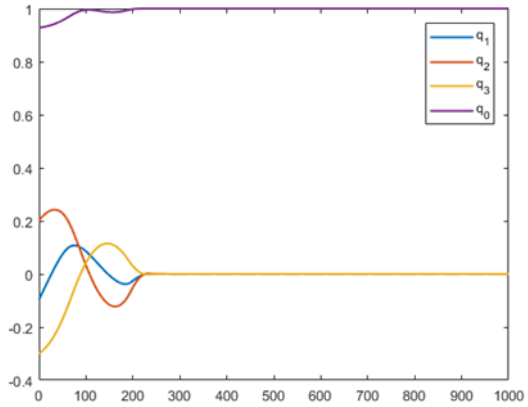

Fig. 7. The quaternion changes on failure mode A

Furthermore, the orbital motion of the solar sail under failure mode A is demonstrated as follows:

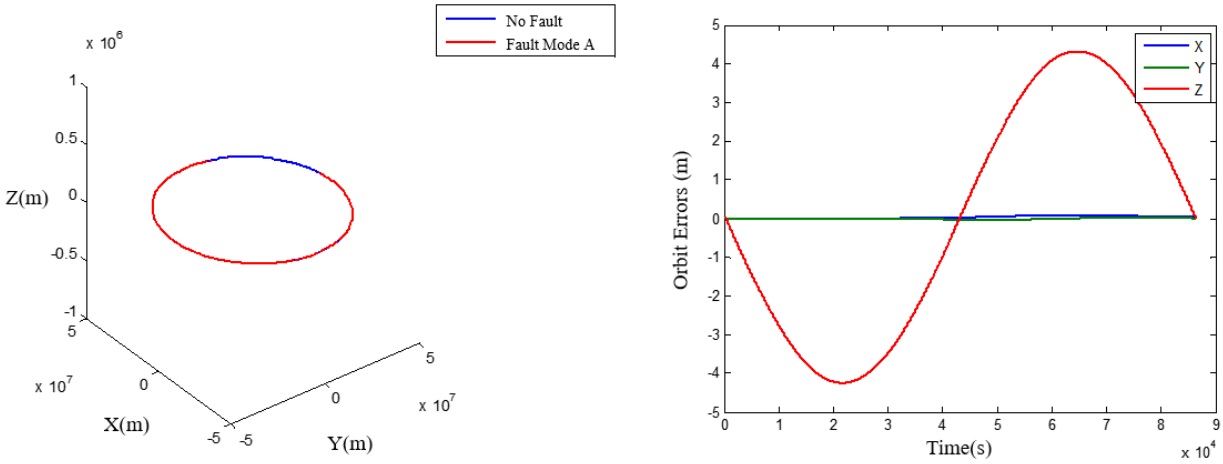

Fig. 8. The 3-D trajectory and orbital errors under faulty mode A

For a solar sail with initial $\boldsymbol{u}_{c0} = [10 \quad 5 \quad 0 \quad 0]^T$ that in accordance with the faulty mode B, the following Figs. 9-10 illustrate its attitude variation with the employment of the proposed control scheme:

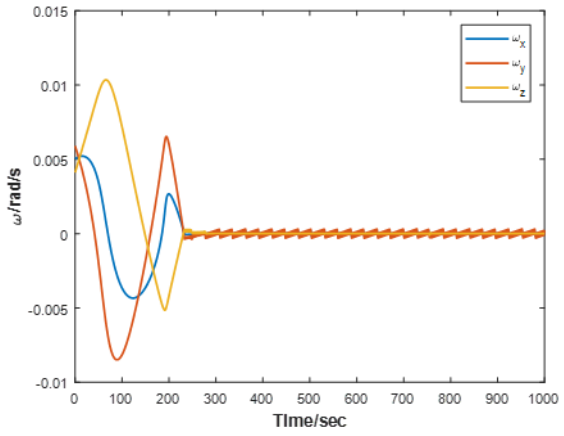

Figure 9: The angular velocity changes on failure mode B

DOI: 10.13009/EUCASS2023-028

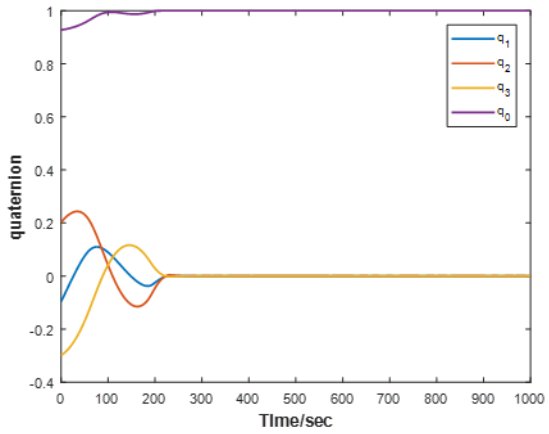

Figure 10: The quaternion changes on failure mode B

Furthermore, the orbital motion of the solar sail under failure mode B is demonstrated as follows:

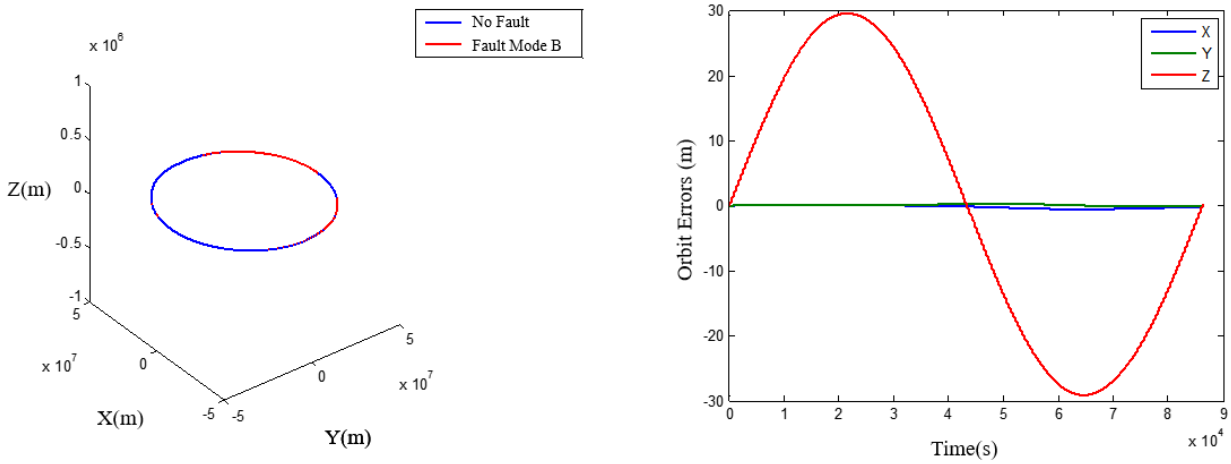

Fig. 11. The 3-D trajectory and orbital errors under faulty mode A

For a solar sail with initial $\boldsymbol{u}_{c0} = [45 \quad 55 \quad 0 \quad 0]^T$ that in accordance with the faulty mode C, the following Figs. 12-13 illustrate its attitude variation with the employment of the proposed control scheme:

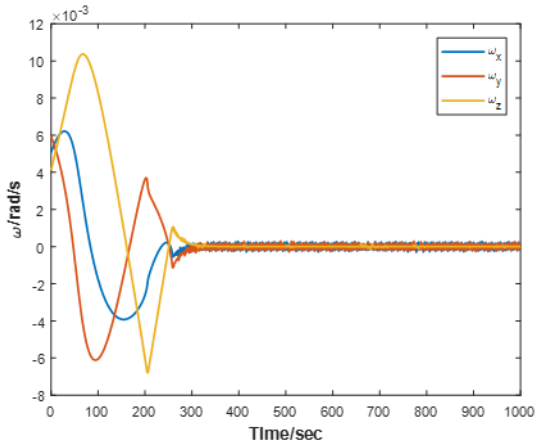

Figure 12: The angular velocity changes on failure mode C

DOI: 10.13009/EUCASS2023-028

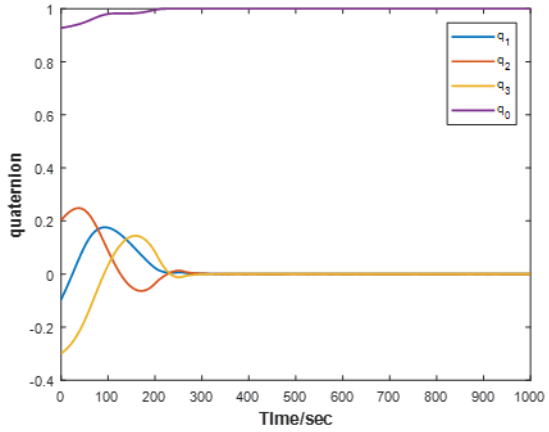

Figure 13: The quaternion changes on failure mode C

Furthermore, the orbital motion of the solar sail under failure mode C is demonstrated as follows:

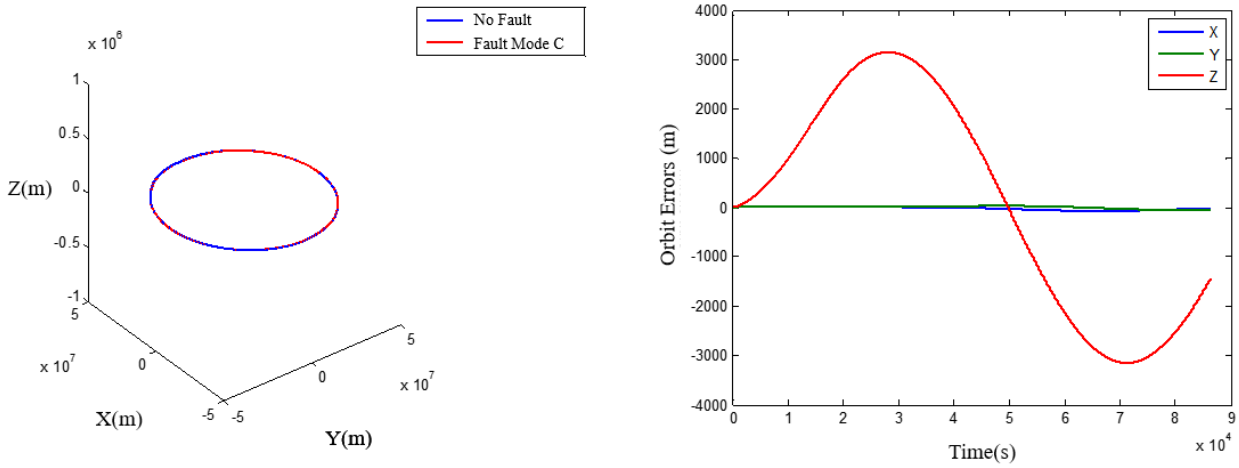

Fig. 14. The 3-D trajectory and orbital errors under faulty mode C

For a solar sail with initial $\boldsymbol{u}_{c0} = [10 \quad 10 \quad 0 \quad 0]^T$ that in accordance with the faulty mode C, the following Figs. 15-16 illustrate its attitude variation with the employment of the proposed control scheme:

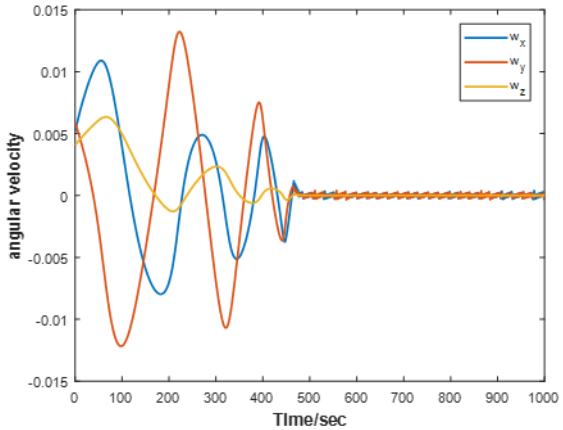

Figure 15: The angular velocity changes on failure mode D

DOI: 10.13009/EUCASS2023-028

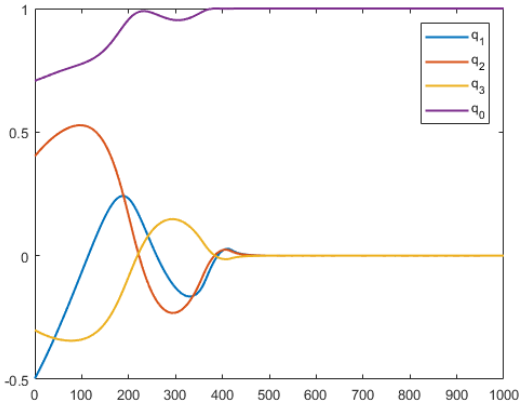

Figure 16. The quaternion changes on failure mode D

Furthermore, the orbital motion of the solar sail under failure mode D is demonstrated as follows:

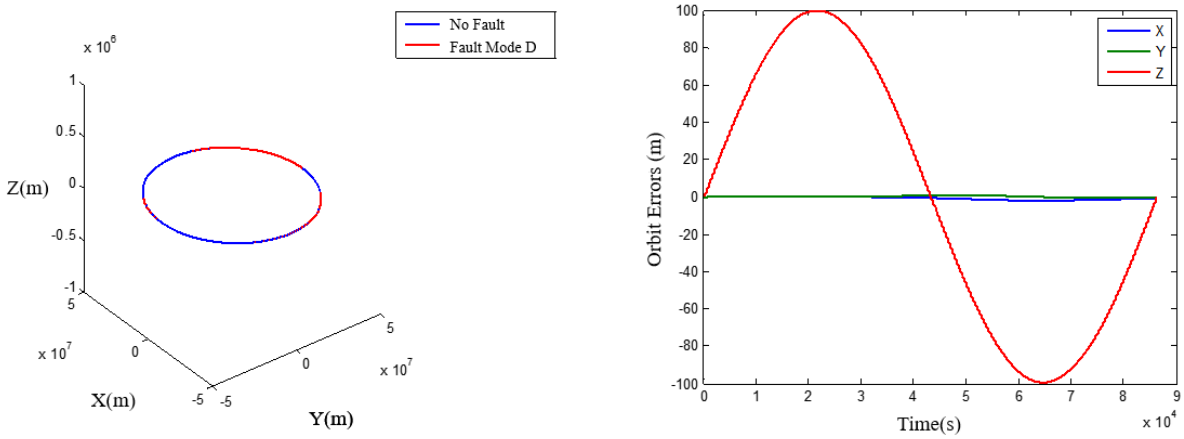

Fig. 17. The 3-D trajectory and orbital errors under faulty mode D

Comparing Fig. 6 with Fig. 12 leads to a conclusion that when the RCD is damaged too much, the FTC can maintain the attitude stability but the angular velocity jitter is more violent. Comparing Fig. 10 and Fig. 17, it can be found that the time required for attitude stabilization is longer than that for non-replaceable type failure when RCD has a replaceable type failure. For Fig. 7, Fig. 10 and Fig. 13, the time required for attitude stabilization is not much different, indicating that the solar sail attitude control can be basically satisfied by RCDs alone with small attitude errors. Besides, the numerical simulation in harmony with the orbital motion demonstrates that the faulty RCDs will deviate the solar sail away from the normal orbit a lot, while the orbital errors are acceptable if the proposed fault-tolerant control scheme is performed to cope with the malfunction in time.

6. Conclusions

In this paper, an active FTC design was developed for the actuator RCDs of a solar sail that suffering from actuator faults. Subsequently, based on the estimated information about actuator faults, FTC law was synthesized to accommodate actuator faults and saturation constraints. The effectiveness of the proposed FTC approach has been illustrated by simulation results, the attitude of the malfunctioned solar sail is stabilized, and the orbital errors resulting from the faulty RCDs are restricted within an acceptable area. Considering that control chattering is observed in the attitude control, further work may be conducted to deal with the control chattering. Besides, the different malfunction of RCDs were divided into 4 different faulty modes by employing the proposed quick inspection approach, while the parameters selection in corresponding to different faulty modes is quite different without a definite criterion or a

DOI: 10.13009/EUCASS2023-028

guideline. Thus, another further work will be the appropriate design of autonomous parameters selection system for a malfunctioning solar sail. Moreover, an orbit-attitude observer-based fault-tolerant control scheme will be investigated in the further work in case of the faulty scenario that no signals can be transmitted from the RCDs to the controller.

References

[1] J. Wang, and X. Wen. 2016. Research status and progress of fault diagnosis technology for spacecraft. Aero Weaponry, 5:71-76.
[2] M. N. Hasan, M. Haris, and S. Qin. 2022. Fault-tolerant spacecraft attitude control: A critical assessment. *Progress in Aerospace Sciences*. 130:100806.
[3] J. K. Wayer, J. F. Castet, and J. H. Saleh, 2013. Spacecraft attitude control subsystem: Reliability, multi-state analyses, and comparative failure behavior in LEO and GEO. *Acta Astronautica*. 85:83-92.
[4] R. Shen, and Y. Zong. 2015. On-orbit fault statistical analysis for remote sensing satellite. *Spacecraft Environment Engineering*. 32(3): 324-329.
[5] T. Hu, S. Gong, J. Mu, J. Li, T. Wang, and W. Qian, 2016. Switch programming of reflectivity control devices for the coupled dynamics of a solar sail. *Advances in Space Research*. 57(5):1147-1158.
[6] V. Manu, N. Balan, Q. Zhang and Z. Xing. 2023. Double superposed epoch analysis of geomagnetic storms and corresponding solar wind and IMF in solar cycles 23 and 24. *Space Weather*. 21(3):2022SW003314.
[7] W. Wang, G. Mengali, A. A. Quarta, and H. Baoyin. 2020. Decentralized fault-tolerant control for multiple electric sail relative motion at artificial Lagrange points. *Aerospace Science and Technology*. 103:105904.
[8] Y. Han, J. D. Biggs, and N. Cui. 2015. Adaptive fault-tolerant control of spacecraft attitude dynamics with actuator failures. *Journal of Guidance, Control, and Dynamics*. 38(10):2033-2042.
[9] Y. Xing, H. Wu, X. Wang, and Z. Li. 2003. Survey of fault diagnosis and fault-tolerance control technology for spacecraft. *Journal of Astronautics*. 24(3):221-226.
[10] S. Yin, B. Xiao, S. Ding, and D. Zhou. 2016. A review on recent development of spacecraft attitude fault tolerant control system. *IEEE Transactions on Industrial Electronics*. 63(5):3311-3320.
[11] P. Martella, A. Tramutola, and M. Montagna. 2001. Fine gyroless attitude control: The SAX experience. *IFAC Proceedings Volumes*. 34(15):37-46.
[12] G. A. Macala, A. Lee, and E. Wang. 2014. Feasibility study of two cassini reaction wheel/thruster hybrid controllers. *Journal of Spacecraft and Rockets*. 51(2):574-585.
[13] J. W. Kruk, B. F. Class, D. Rovner, J. Westphal, T. B. Ake, H. W. Moos, B. A. Roberts, and L. Fisher. 2003. FUSE in-orbit attitude control with two reaction wheels and no gyroscopes. *Future EUV/UV and Visible Space Astrophysics Missions and Instrumentation*. 4854:274-285.
[14] M. N. Sweeting, Y. Hashida, N. P. Bean, M. S. Hodgart, and H. Steyn. 2004. CERISE microsatellite recovery from first detected collision in low Earth orbit. *Acta Astronautica*. 55(2):139-147.
[15] A. de Ruiter, 2011. A fault-tolerant magnetic spin stabilizing controller for the JC2Sat-FF mission. *Acta Astronautica*. 68(1-2):160-171.
[16] M. Wang, and Y. Xie, 2010. Spacecraft thrusters real time command allocation algorithm in consideration of thrust upper bounds and thruster failures. *Journal of Astronautics*. 31(6): 1540-1546.
[17] Y. Zhang, F. Yu, Y. Zheng, Z. Huang, L. Chen, and Z. Jin. 2007. Fault tolerance design of pico-satellite's housekeeping system. *Journal of Astronautics*. 28(6): 1753-1757.